Bruno Botta,[a] Caterina Fraschetti,[a] Ilaria D'Acquarica,[a] Fabiola Sacco,[a]

Jochen Mattay,[b] Matthias C. Letzel,[b] and Maurizio Speranza.[a]*

Unprecedented Gas-Phase Chiroselective Logic Gates.

SUPPORTING INFORMATION

- Experimental section
- Ion abundances and kinetic plots of the gas-phase reaction between diastereomeric $[M \cdot H \cdot N]^+$ complexes and B (M: either 1^R or 1^S; N: 2-5; B: either B^R or B^S) (Figures S1-S15).
- Reaction mechanism and kinetic treatment of data.
- Rate constants of the reaction between the $[1^R \cdot H \cdot N]^+$ and $[1^S \cdot H \cdot N]^+$ diastereoisomers ad the 2-aminobutane enantiomers (B^R and B^S).

Experimental Section.

.

Materials. Enantiomerically pure basket-type resorcin[4]arenes, either in the *all-R* configuration (1^R) or in the *all-S* one (1^S), in their flattened-cone conformations, were synthesized and purified according to established procedures.[a] Cytarabine (2), gemcitabine hydrochloride (3•HCl), 2'-deoxycytidine (4), and cytidine (5) were purchased from commercial sources and used without further purification. The same source provided the (*R*)-(-)- (B^R) and (*S*)-(+)-2-aminobutane (B^S), which were purified in the vacuum manifold with several freeze-thaw cycles.

[a] B. Botta, I. D'Acquarica, L. Nevola, F. Sacco, Z. Valbuena Lopez, G. Zappia, C. Fraschetti, M. Speranza, A. Tafi, F. Caporuscio, M. C. Letzel, J. Mattay, *Eur. J. Org. Chem.* 2007, **36**, 5995-6002.

Nano-ESI-FT-ICR experiments. The experiments were performed at room temperature in an APEX III FT-ICR mass spectrometer fitted with a nano-ESI source (Apollo Bruker) and a resonance cell ("infinity cell") located between the poles of a superconducting magnet (7.0 T). Stock CH_3OH solutions of the enantiomerically pure resorcin[4]arenes (either 1^R or 1^S; 1×10^{-5} M), each containing a twofold excess of the nucleoside (N=2, 3, 4, or 5) were electrosprayed through a capillary (dry gas N_2: 50°C) into the external source of the FT-ICR mass spectrometer. The resulting ions were transferred into the

resonance cell by use of a system of potentials and lenses and were quenched by collisions with argon pulsed into the cell through a magnetic valve. Depending upon the configuration of the resorcin[4]arene, whether $\mathbf{1^R}$ or $\mathbf{1^S}$, and the nature of N, nano-electrospray ionization (nano-ESI) of the above methanolic solutions leads to the formation of the corresponding proton-bound complex, either $[\mathbf{1^R \cdot H \cdot N}]^+$ or $[\mathbf{1^S \cdot H \cdot N}]^+$. The complex was monitored and isolated by broad-band ejection of the accompanying ions and ,then, allowed to react with the chiral amine B (either $\mathbf{B^R}$ or $\mathbf{B^S}$), present in the cell at a fixed pressure P (from 1.2×10^{-8} to 6.2×10^{-8} mbar) (Figures S2-S15 below).

Kinetic Plots. The time-dependent decay of the $[\mathbf{1^R \cdot H \cdot N}]^+$ or $[\mathbf{1^S \cdot H \cdot N}]^+$ reactants was monitored by measuring its intensity (I) at any delay time t relative to that at $t=0$ (I^0), calculated as the sum of I and of the intensities of the addition (I_{add}) and substitution (I_{exc}) products. The dependence of $\ln[I/(I+I_{add}+I_{exc})]$ vs t is not linear, as expected for simple parallel or consecutive reaction patterns, but invariably exhibits a curvature towards an asymptotic limit, different for each system (Figure S1).


Figure S1. Time-dependent decay curves of $[\mathbf{1^S \cdot H \cdot N}]^+$.
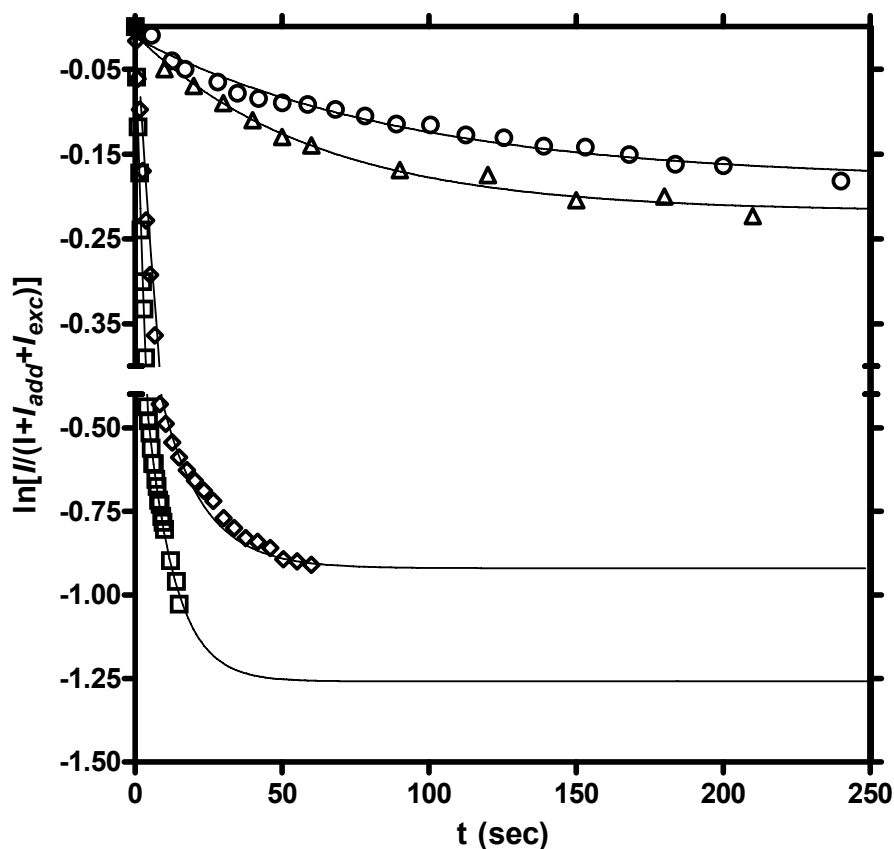
Figure S1. Time-dependent decay of $[\mathbf{1^S \cdot H \cdot N}]^+$ (N=**2** (triangles; P(**B^S**) = 4.4×10^{-8} mbar), **3** (diamonds; P(**B^S**) = 1.4×10^{-8} mbar), **4** (circles; P(**B^S**) = 4.0×10^{-8} mbar), and **5** (squares; P(**B^S**) = 4.5×10^{-8} mbar). Qualitatively similar trends have been observed with $[\mathbf{1^R \cdot H \cdot N}]^+$ (N = **2**, **3**, and **5**). No decay of $[\mathbf{1^R \cdot H \cdot 4}]^+$ has been observed even after 300 s reaction time ([B] = 7.4×10^9 molecule cm^{-3}).

Figures S2-S15. Kinetic plots: open circles (starting complex); triangles (its adduct with B); full circles (B-to-N substitution product). The pressure indicated in the captions refers to the presence of the 2-aminobutane enantiomer employed, either B^R or B^S. The continuous lines represent the relative abundance of reactants and products calculated from the exact rate expressions (a)-(c) for network (1) (see below).


Figure S2. $[1^R \cdot H \cdot 2]^+ + B^R$ (P=6.2x10^{-8} mbar)
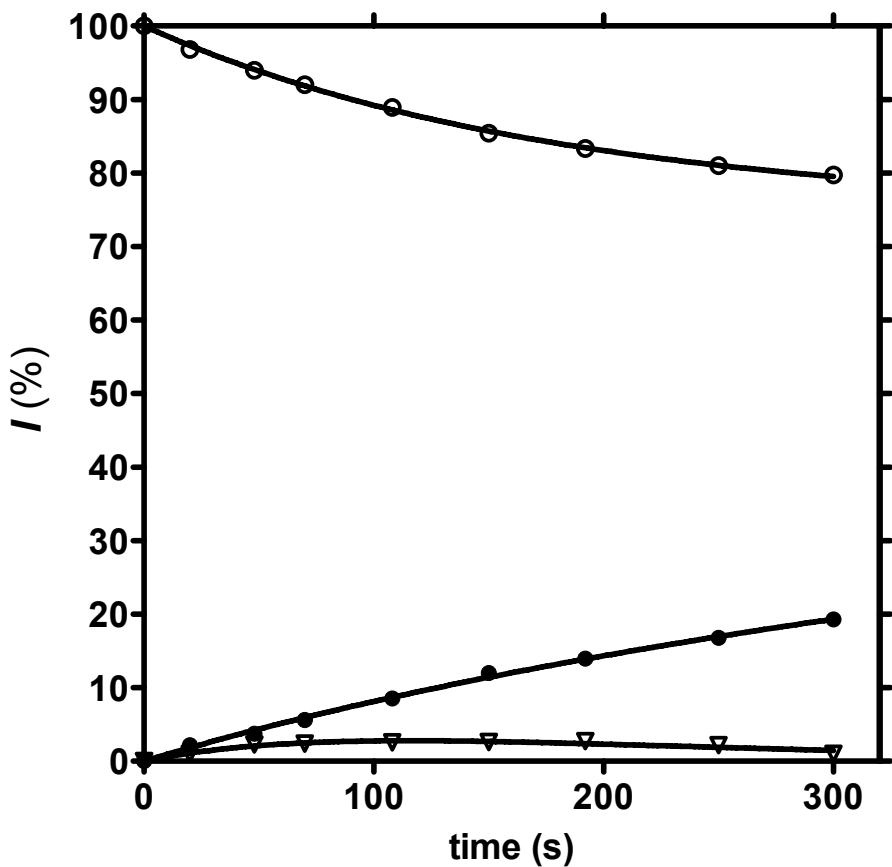
Figure S3. $[\mathbf{1}^R \cdot H \cdot \mathbf{2}]^+ + \mathbf{B}^S$ (P= 4.1×10^{-8} mbar)
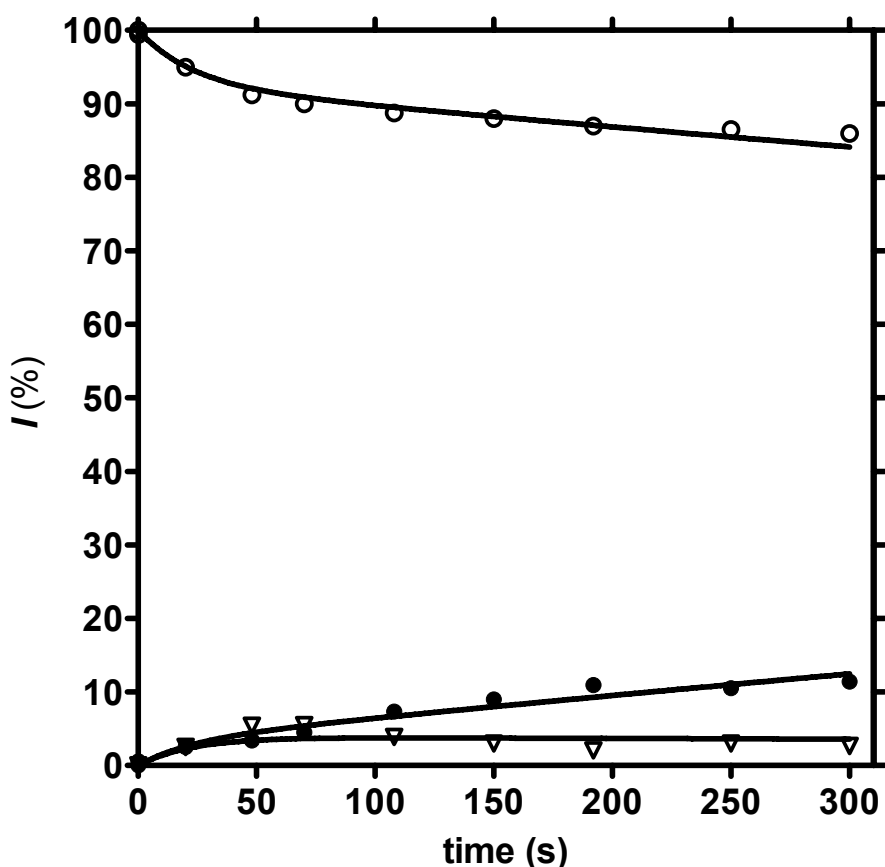
Figure S4. $[1^R \cdot H \cdot 3]^+ + B^R$ (P= 1.2×10^{-8} mbar)
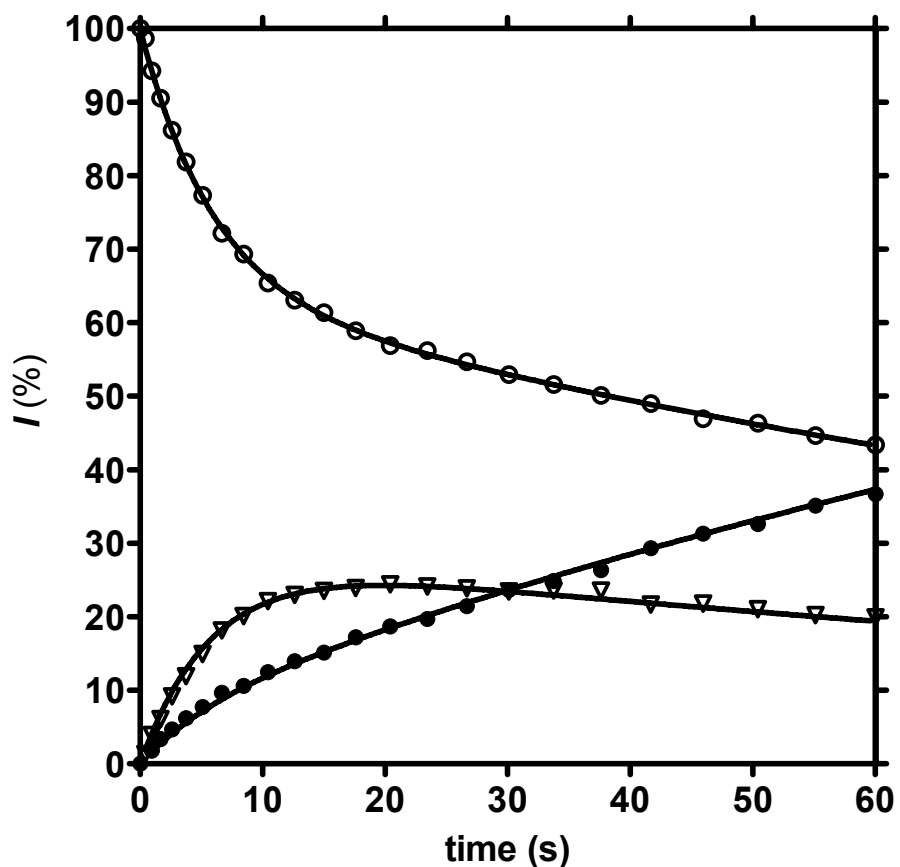
**Figure S5.** $[1^R \cdot H \cdot 3]^+ + B^S$ (P= 1.3×10^{-8} mbar)
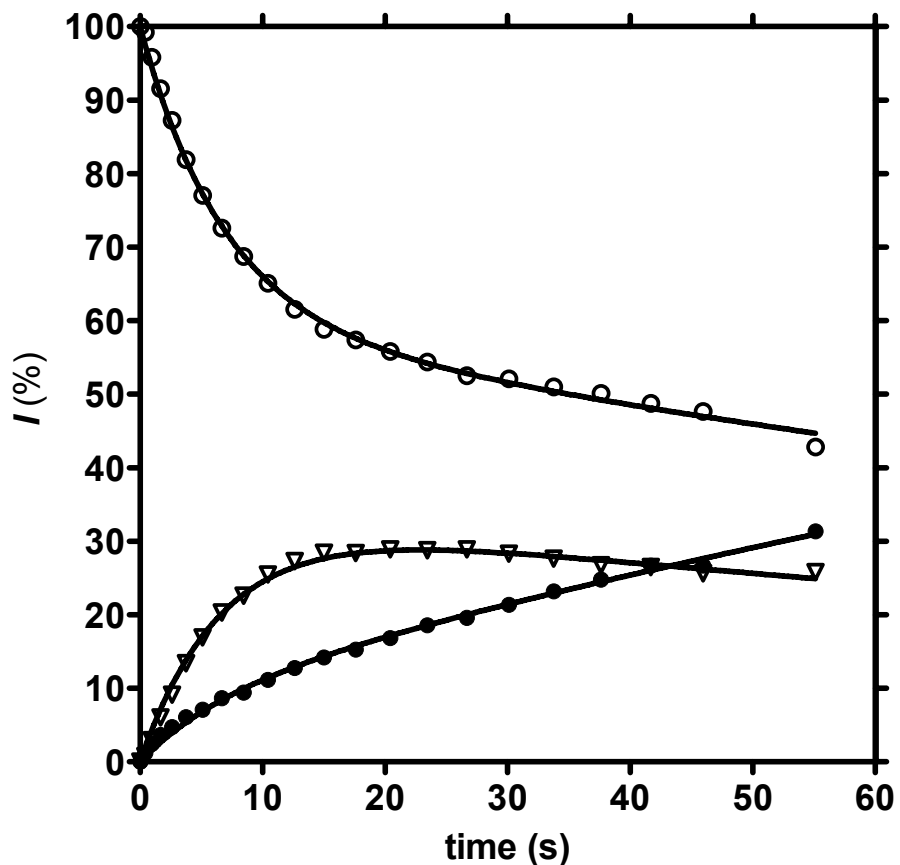
Figure S6. $[\mathbf{1^R \cdot H \cdot 5}]^+ + \mathbf{B^R}$ (P= 4.0×10^{-8} mbar)
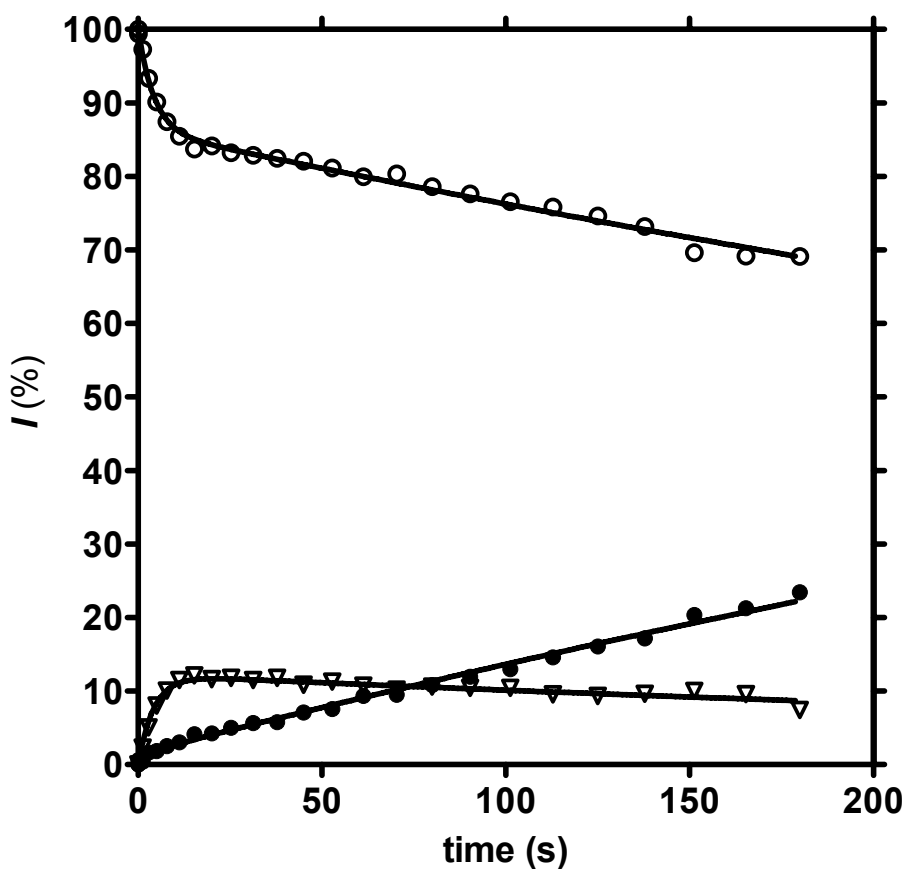
Figure S7. $[1^R \cdot H \cdot 5]^+ + B^S$ (P= 4.5×10^{-8} mbar)
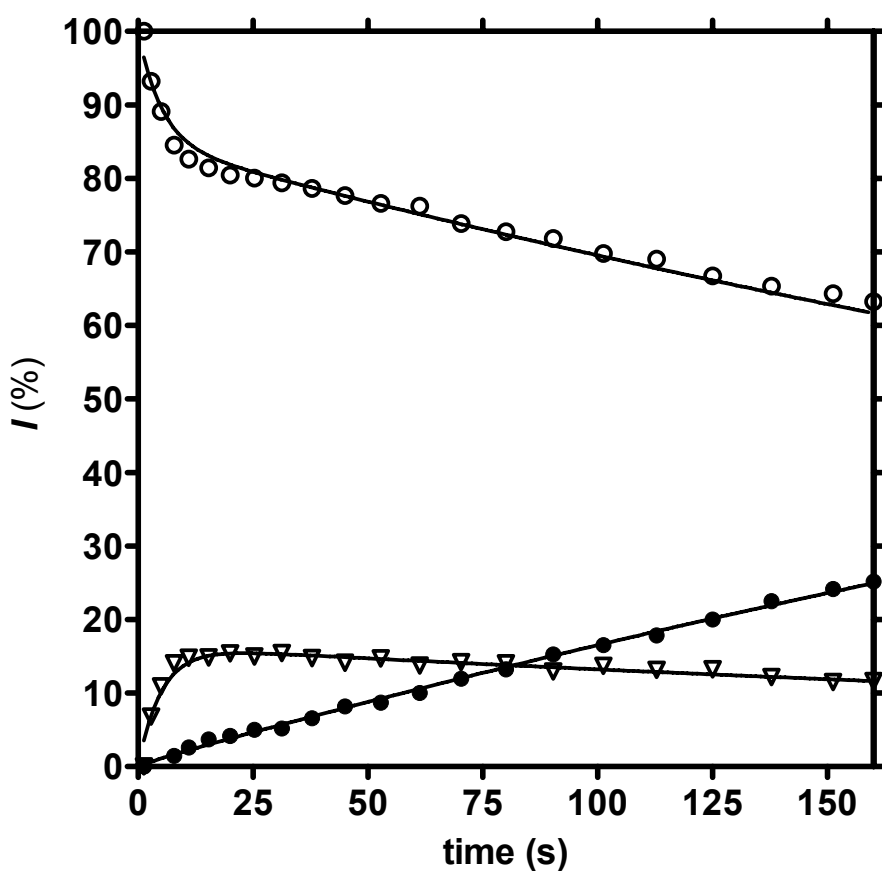
**Figure S8.** $[1^S \cdot H \cdot 2]^+ + B^R$ (P= 6.2×10^{-8} mbar)
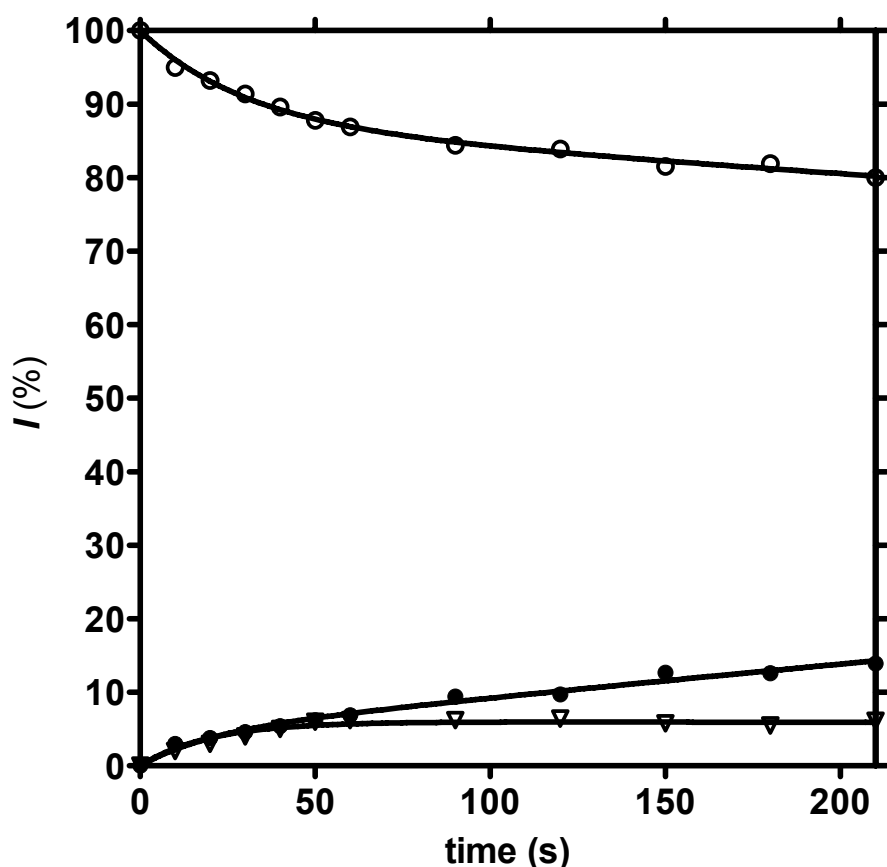
Figure S9. $[\mathbf{1^S \cdot H \cdot 2}]^+ + \mathbf{B^S}$ (P= 4.4×10^{-8} mbar)
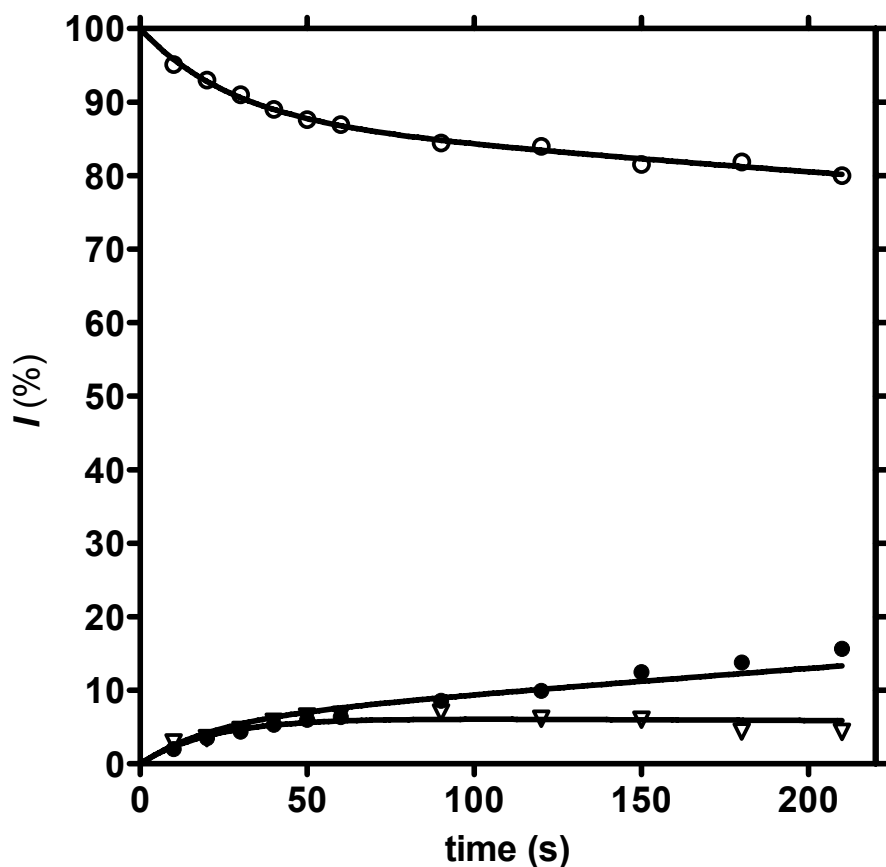
Figure S10. $[1^S \cdot H \cdot 3]^+ + B^R$ (P= 4.0×10^{-8} mbar)
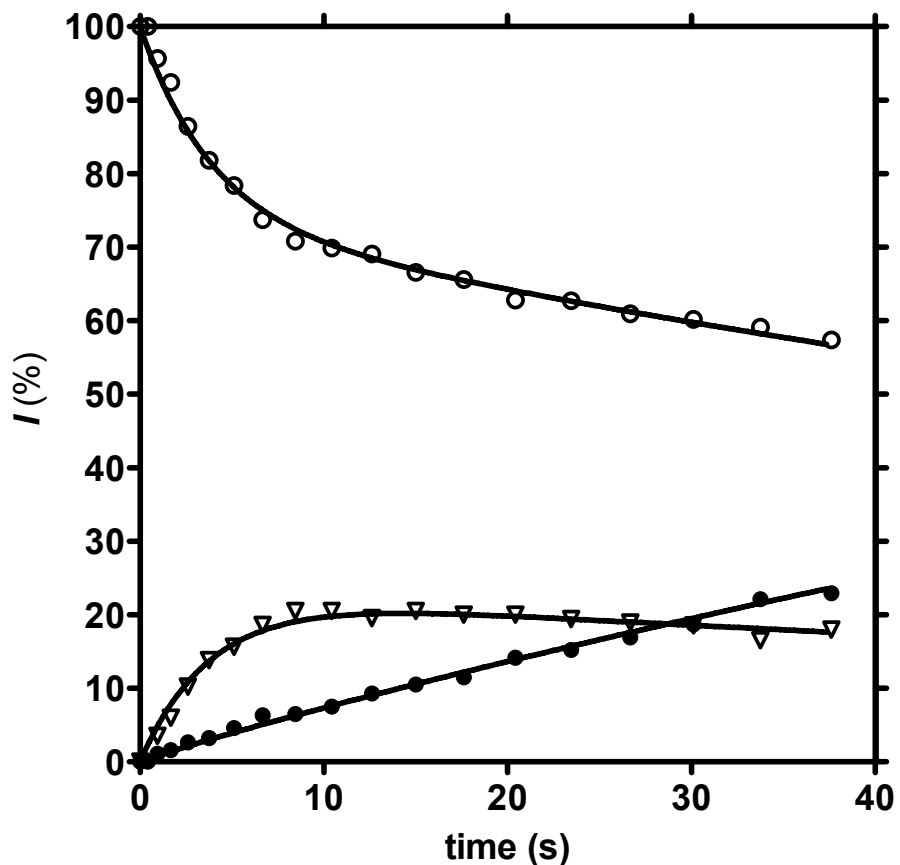
Figure S11. $[1^S \cdot H \cdot 3]^+ + B^S$ (P= 1.4×10^{-8} mbar)
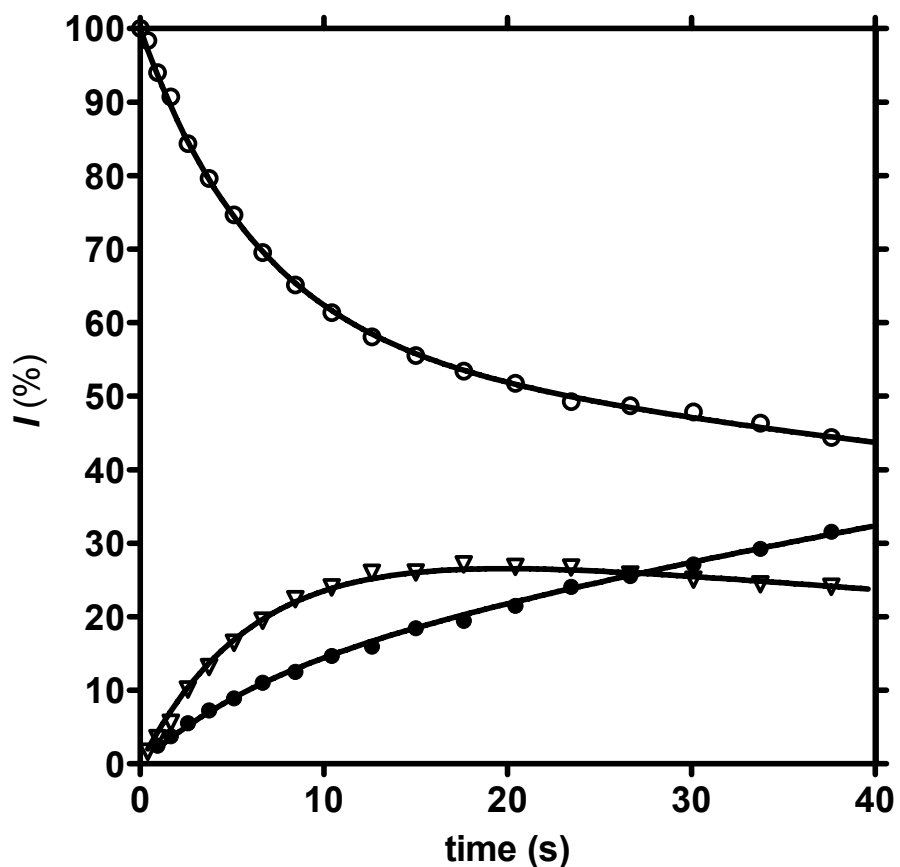
Figure S12. $[1^S \cdot H \cdot 4]^+ + B^R$ (P= 4.2×10^{-8} mbar)
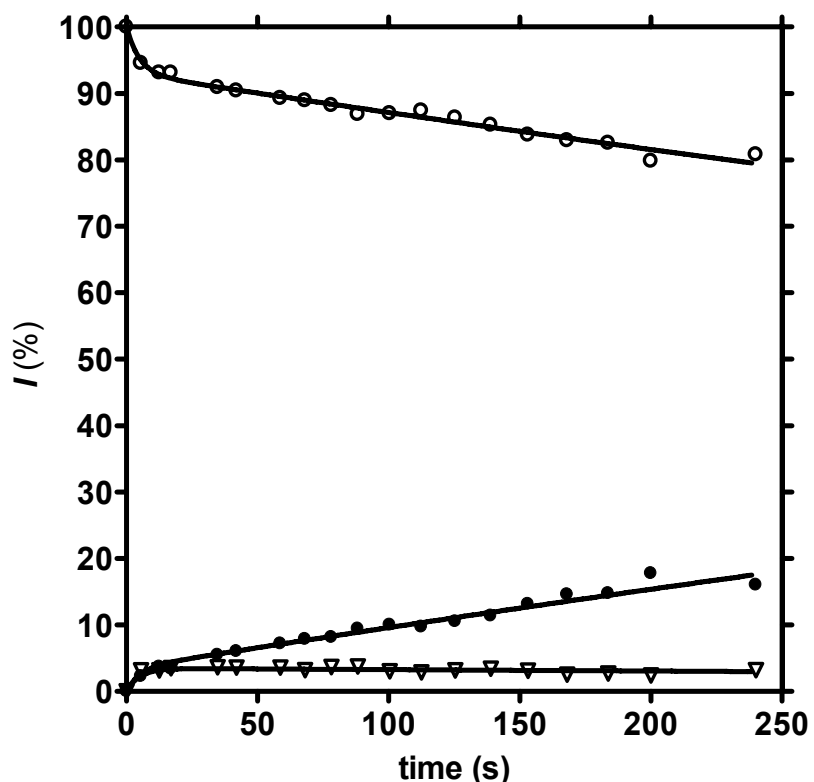
Figure S13. $[1^S \cdot H \cdot 4]^+ + B^S$ (P= 4.0x10^{-8} mbar)
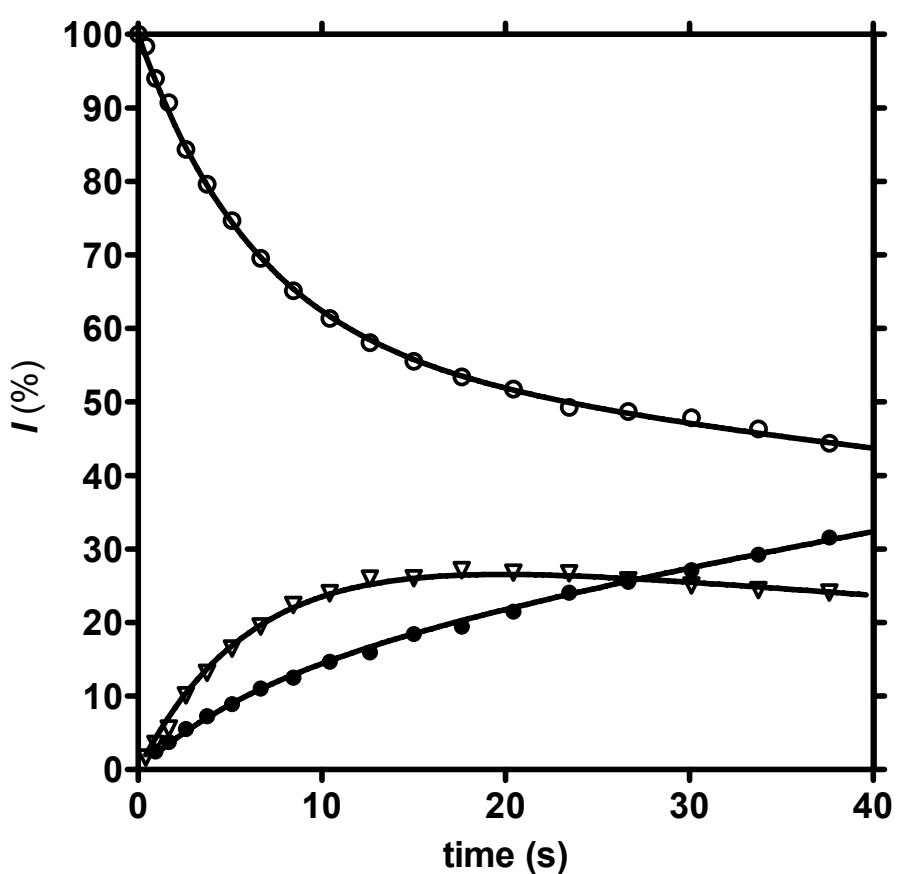
Figure S14. $[1^S \cdot H \cdot 5]^+ + B^R$ (P= 4.0×10^{-8} mbar)
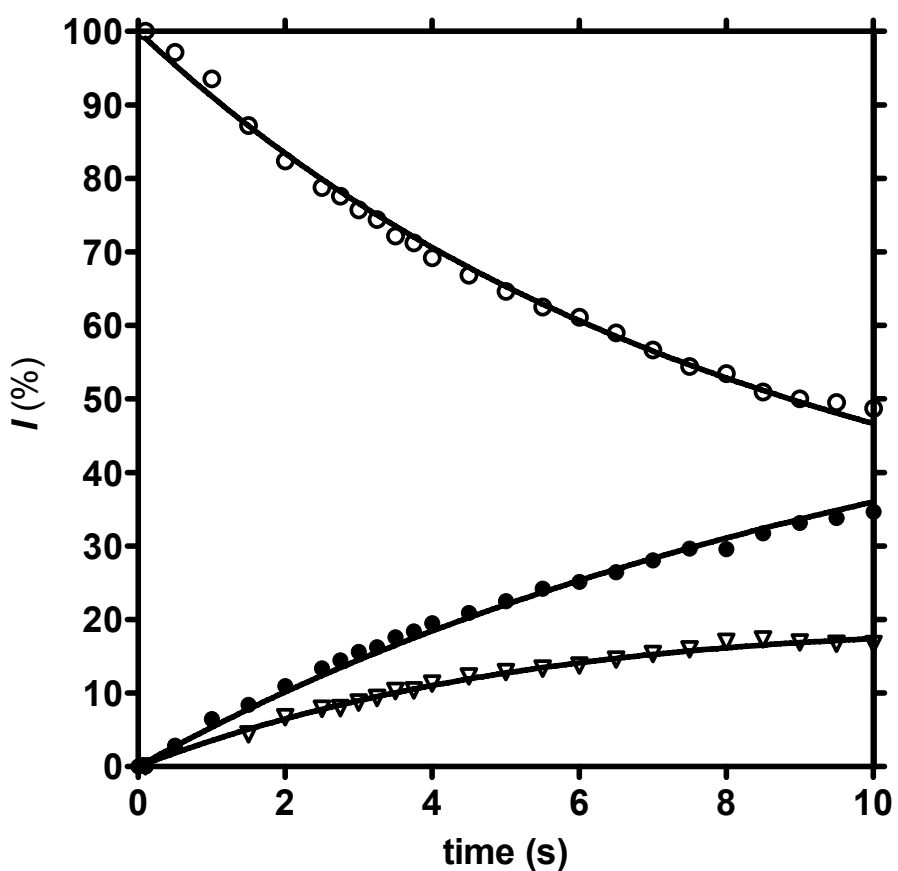
Figure S15. $[1^S \cdot H \cdot 5]^+ + B^S$ (P= 4.5×10^{-8} mbar)
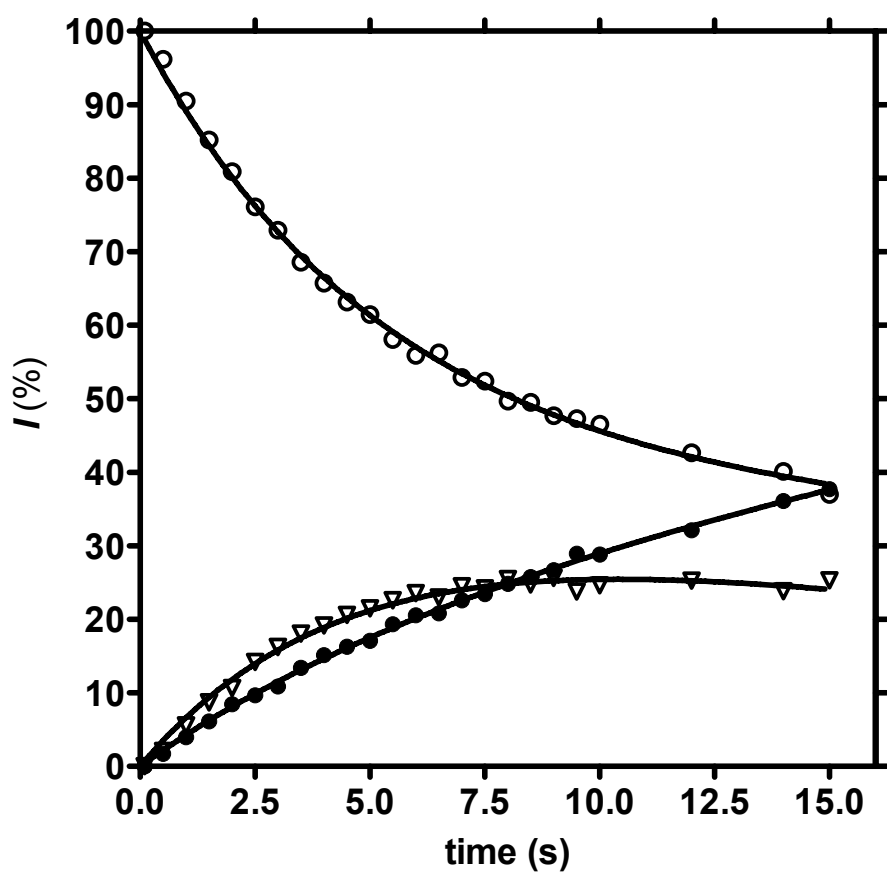
*Reaction mechanism and kinetic equations.* According to Figures S1-S15, reaction 1 obeys the following reaction mechanism (M: either 1^R or 1^S; N: 2-5; B: either B^R or B^S):

$$[M•H•N]^+ + B \underset{k_{-1}}{\overset{k_1}{\rightleftharpoons}} [M•H•N•B]^+ \overset{k_2}{\longrightarrow} [M•H•B]^+ + N \qquad (1)$$
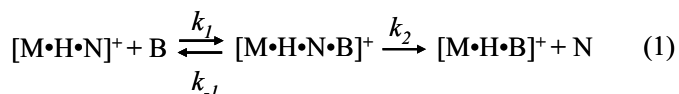
Application of the steady-state approximation and the pre-equilibrium approximation to the above kinetic sequence is excluded on the grounds of the sizable time-dependent amounts of the $[M•H•N•B]^+$ intermediate (Figures S2-S15). However, given the large excess of the amine B in the FT-ICR cell, relative to the $[M•H•N]^+$ concentration, each step of the reaction network can be considered as a pseudo-first-order transformation. In this case, the difficult task of solving simultaneous differential equations that describe the exact rate expressions for each chemical species involved in the sequence can be efficiently solved by a Laplace transform pair.[b] Taking into account that, at $t = 0$, neither $[M•H•N•B]^+$ nor $[M•H•B]^+$ are present in the FT-ICR reaction cell ($I^0_{add} = I^0_{exc} = 0$), the time-dependence of the chemical species of the sequence can be expressed as:

$$I = \frac{I^0}{\gamma_2 - \gamma_1}\left[(k_2 + k_3 - \gamma_1)e^{-\gamma_1 t} - (k_2 + k_3 - \gamma_2)e^{-\gamma_2 t}\right] \qquad \text{for } [M•H•N]^+ \qquad (a)$$

$$I_{exc} = \frac{I^0 k'_1}{\gamma_2 - \gamma_1}\left[e^{-\gamma_1 t} - e^{-\gamma_2 t}\right] \qquad \text{for } [M•H•N•B]^+ \qquad (b)$$

$$I_{add} = I^0\left[1 + \frac{k'_1 k_3}{\gamma_1(\gamma_1 - \gamma_2)}e^{-\gamma_1 t} + \frac{k'_1 k_3}{\gamma_2(\gamma_2 - \gamma_1)}e^{-\gamma_2 t}\right] \qquad \text{for } [M•H•B]^+ \qquad (c)$$

with: $\gamma_1 \gamma_2 = k'_1 k_3$ and $\gamma_1 + \gamma_2 = k'_1 + k_2 + k_3$. Best fit of the kinetic equations a-c with the experimental kinetic data experimental results allows extraction of the first-order kinetic constants k'_1, k_2, and k_3. The first-order parameter k'_1 can be eventually converted into the corresponding second-order constant $k_1 = k'_1/[B]$. The values of k_1, k_2, and k_3 are reported in Table S1.

Table S1. Rate Constants of the Reaction between the $[1^R•H•N]^+$ and $[1^S•H•N]^+$ Diastereoisomers ad the 2-Aminobutane Enantiomers (B^R and B^S).

N	Rate Const.[a]	$[1^R•H•N]^+$ B=B^R	$[1^S•H•N]^+$ B=B^R	$[1^R•H•N]^+$ B=B^S	$[1^S•H•N]^+$ B=B^S
2	$10^{12}k_1$	0.10±0.03	0.47±0.04	0.22±0.05	0.35±0.05
	$10^2 k_{-1}$	0.42±0.04	4.18±0.45	4.08±0.02	4.07±0.49
	$10^2 k_2$	0.09±0.02	0.55±0.12	0.19±0.05	0.32±0.02
3	$10^{12}k_1$	20.60±4.96	8.24±0.76	21.30±4.18	7.17±0.91
	$10^2 k_{-1}$	11.22±0.39	19.36±0.10	9.10±0.71	9.40±0.38
	$10^2 k_2$	1.81±0.03	0.87±0.05	1.71±0.05	2.29±0.02
4	$10^{12}k_1$	<0.01	0.94±0.03	<0.01	0.56±0.02
	$10^2 k_{-1}$		18.82±0.77		11.23±0.03
	$10^2 k_2$		0.75±0.04		0.46±0.09
	$10^{12}k_1$	3.60±0.42	4.84±0.57	4.04±0.48	9.39±1.10

5	10^2k_{-1}	20.25±2.13	7.56±0.07	16.82±0.07	9.53±1.41
	10^2k_2	0.47±0.05	5.63±0.05	0.24±0.03	4.53±0.07

[a] k_1 in cm^3 molecule^{-1} s^{-1}; k_{-1} and k_2 in s^{-1}.

[b] J. Andraos, *J. Chem. Educ.*, 1999, **76 (11)**, 1578-1583.